the FEBS Journal

Dual role of oxygen during lipoxygenase reactions

Igor Ivanov[1,2], Jan Saam[1], Hartmut Kuhn[1] and Hermann-Georg Holzhütter[1]

1 Institute of Biochemistry Humboldt University Medical School Charité, Berlin, Germany
2 M.V. Lomonosov State Academy of Fine Chemical Technology, Moscow, Russian Federation

Keywords
atherosclerosis; eicosanoids; enzymology; inflammation; osteoporosis; reaction kinetics

Correspondence
H.-G. Holzhütter, Institute of Biochemistry, Charité–University Medicine Berlin, Monbijoustr. 2, 10117 Berlin, Germany
Fax: +49 30 450 528905
Tel: +49 30 450 528040
E-mail: hergo@charite.de

(Received 8 February 2005, revised 7 March 2005, accepted 21 March 2005)

doi:10.1111/j.1742-4658.2005.04673.x

Studying the oxygenation kinetics of (19*R/S*,5*Z*,8*Z*,11*Z*,14*Z*)-19-hydroxyeicosa-5,8,11,14-tetraenoic acid (19-OH-AA) by rabbit 15-lipoxygenase-1 we observed a pronounced oxygen dependence of the reaction rate, which was not apparent with arachidonic acid as substrate. Moreover, we found that peroxide-dependent activation of the lipoxygenase depended strongly on the oxygen concentration. These data can be described with a kinetic model that extends previous schemes of the lipoxygenase reaction in three essential aspects: (a) the product of 19-OH-AA oxygenation is a less effective lipoxygenase activator than (13*S*,9*Z*,11*E*)-13-hydroperoxyoctadeca-9,11-dienoic acid; (b) molecular dioxygen serves not only as a lipoxygenase substrate, but also impacts peroxide-dependent enzyme activation; (c) there is a leakage of radical intermediates from the catalytic cycle, which leads to the formation of inactive ferrous lipoxygenase. This enzyme inactivation can be reversed by another round of peroxide-dependent activation. Taken together our data indicate that both peroxide activation and the oxygen affinity of lipoxygenases depend strongly on the chemistry of the lipid substrate. These findings are of biological relevance as variations of the reaction conditions may turn the lipoxygenase reaction into an efficient source of free radicals.

Lipoxygenases (LOXs) form a heterogeneous family of lipid peroxidizing enzymes that catalyse dioxygenation of free and/or esterified polyunsaturated fatty acids to their corresponding hydroperoxy derivatives [1]. In mammals, LOXs are categorized with respect to their positional specificity of arachidonic acid oxygenation into 5-, 8-, 12- and 15-LOXs [2], but plant physiologists prefer a linoleic acid related enzyme nomenclature [3]. Mammalian LOXs (EC 1.13.11.33) are involved in the biosynthesis of inflammatory mediators, such as leukotrienes [4] and lipoxins [5], but have also been implicated in cell differentiation [6,7], carcinoma metastasis [8], atherogenesis [9,10] and osteoporosis [11]. 5-LOX inhibitors and leukotriene receptor antagonists have been developed as antiasthmatic drugs and some of them are available for prescription use [12,13].

Mechanistically, the LOX reaction consists of four consecutive steps (Scheme 1): (a) stereo-selective hydrogen abstraction from a bisallylic methylene forming a carbon-centred fatty acid radical; (b) rearrangement of the fatty acid radical, which is bound at the active site as planar pentadienylic intermediate or, more likely, as nonplanar allylic radical [14]; (c) stereo-specific insertion of molecular dioxygen forming an oxygen-centred hydroperoxy radical; (d) reduction of the hydroperoxy fatty acid radical to the corresponding product anion. Although the LOX-reaction involves the formation of radical intermediates it may not be considered an effective source of free radicals as most of the intermediates remain enzyme bound. However, under certain conditions a considerable proportion of radical intermediates may escape the active site [15,16] leaving the enzyme in an inactive ferrous (E^{2+}) form. Thus to keep the reaction at a quasi-stationary level it requires the presence of activating hydroperoxides that are naturally formed as reaction products during the reaction but

Abbreviations
19-OH-AA, (19*R/S*,5*Z*,8*Z*,11*Z*,14*Z*)-19-hydroxyeicosa-5,8,11,14-tetraenoic acid; LOX, lipoxygenase; 13*S*-HpODE: (9*Z*,11*E*, 13*S*)-13-hydroperoxyoctadeca-9,11-dienoic acid; 15-OOH-19-OH-AA, (5*Z*,8*Z*,11*Z*,13*E*,15*S*,19*S/R*)-15-hydroperoxy-19-hydroxyeicosa-5,8,11,13-tetraenoic acid; 13-KODE, 13-keto-(9*Z*,11*E*)-octadecadienoic acid.

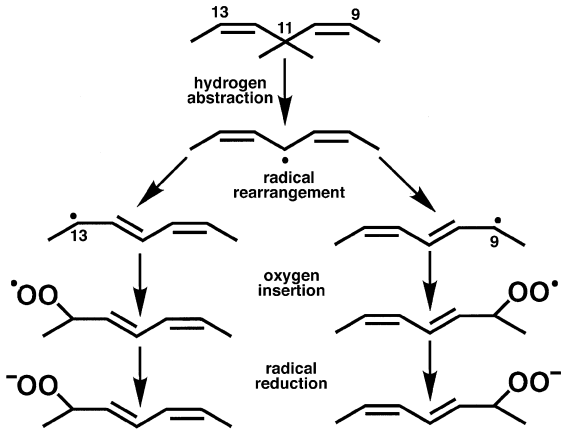

Scheme 1. Radical mechanism of the LOX reaction. The four elementary reaction of the catalytic (hydrogen abstraction, radical rearrangement, oxygen insertion and radical reduction) are shown.

which on top can be added to the reaction mixture. (9*Z*,11*E*, 13*S*)-13-hydroperoxyoctadeca-9,11-dienoic acid (13-HpODE) is such a hydroperoxy fatty acid typically used as exogenous enzyme activator to prevent long and hardly controllable lag phases of the reaction.

The affinity of LOXs for oxygen during fatty acid oxygenation is high. K_M-values for oxygen ranging between 10 and 26 μM have been reported for various LOX isoforms [17]. A rapid diffusion controlled mechanism of oxygen penetration into the active site of the enzyme is generally assumed. However, when we investigated the oxygenation of hydroxylated arachidonic acid isomers (OH-AA) by the rabbit 15-LOX we observed the reaction rate to be strongly oxygen dependent. Moreover, we found that at low oxygen concentrations, high concentrations of hydroperoxy fatty acids were required for maximal activation of the enzyme. In contrast, at greater oxygen concentrations lower hydroperoxide concentrations were sufficient. These findings are not compatible with the conventional model of the LOX reaction, which was based on the assumption that the oxygen concentration does not impact peroxide-dependent enzyme activation [18,19].

To investigate this phenomenon in more detail we studied the kinetics of 15-LOX-catalysed oxygenation of (19*R/S*,5*Z*,8*Z*,11*Z*,14*Z*)-19-hydroxyeicosa-5,8,11,14-tetraenoic acid (19-OH-AA) (Fig. 1), varying the initial concentrations of enzyme, fatty acid substrate, oxygen and peroxide activator. The experimental data were fitted to an extended kinetic scheme of the LOX reaction, which allowed oxygen to impact peroxide-dependent enzyme activation. This kinetic model predicts a biphasic oxygen dependence of the reaction rate with a high and a low-affinity part.

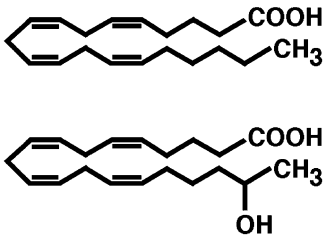

Fig. 1. Chemical structure of arachidonic acid and 19-OH-AA.

Results and Discussion

15-LOX catalysed oxygenation of hydroxylated polyenoic fatty acids

Previous experiments with ω-hydroxylated polyenoic fatty acids indicated ineffective oxygenation of these substrates by the rabbit 15-LOX and basic kinetic characterization revealed a high apparent K_M and a low reaction rate [20]. Here we investigated the oxygenation kinetics of 19-OH-AA in more detail and found that the initial oxygenation rates were strongly augmented at hyperbaric oxygen tensions (Table 1). In contrast, the oxygenation rates of nonhydroxylated polyenoic fatty acids (linoleic acid or arachidonic acid) were hardly impacted. Interestingly, such striking oxygen dependence was not observed when the methyl esters of the hydroxy fatty acids were used as substrate (Table 1). Analysis of the reaction products (see supplementary material) indicated predominant n-6-lipoxygenation of both polyenoic fatty acids and their hydroxy derivatives. However, hydroxy fatty acid methyl esters were oxygenated at C-5 of the hydrocarbon backbone (Table 1). Taken together, the experimental data suggest that presence of a hydroxy group alters the oxygen dependence of the reaction. In fact, when hydroxy fatty acids were oxygenated under normoxic conditions the oxygen concentration was rate limiting, but this was not the case for the nonhydroxylated substrates. Interestingly, this rate limitation could not be overcome even at very high oxygen concentration (> 800 μM) suggesting a nonsaturable component of oxygen supply.

Spectrophotometric progress curves of conjugated diene formation

We carried out spectrophotometric measurements of 15-LOX-catalysed oxygenation of 19-OH-AA varying the initial concentrations of fatty acid substrate, oxygen, enzyme and 13*S*-HpODE used as enzyme activator. In these experiments enzyme concentrations were

Table 1. Relative reaction rates of 15-LOX catalysed oxygenation of polyenic fatty acid derivatives. The oxygenation rates of the different fatty acid derivatives were determined spectrophotometrically as described in Experimental procedures. The substrate concentration was at least fivefold greater than the apparent K_m value estimated under normoxic conditions. The absolute rates measured under normoxic condition for each substrate were set 100%. Hyperoxic conditions indicate that the reactions were carried out in oxygen flushed reaction buffer. In a separate experiment (oxygraphic assay) we determined an oxygen concentration of ≈0.95 mM under these conditions. The structures of the oxygenation products were determined by RP-HPLC, SP-HPLC, chiral phase-HPLC, UV-spectroscopy and GC/MS.

Fatty acid	Normoxic conditions (%)	Hyperoxic conditions (%)	Position of major oxygenation
Arachidonic acid	100	99 ± 7[a]	C-15 (n-6)
Linoleic acid	100	91 ± 18[a]	C-13 (n-6)
ω-hydroxy arachidonic acid	100	270 ± 11[b]	C-15 (n-6)
ω-hydroxy linoleic acid	100	245[c]	C-13 (n-6)
19-OH-AA	100	200 ± 65[b]	C-15 (n-6)
Methyl ω-hydroxy arachidonate	100	101 ± 10[b]	C-5
Methyl 19-OH-AA	100	105 ± 10[b]	C-5

[a] $n = 3$, [b] $n = 2$, [c] $n = 1$.

kept sufficiently low so as to prevent notable decreases in substrate concentration (oxygen and 19-OH-AA) during the entire measuring period. From Fig. 2A–D it can be seen that irrespective of the starting conditions all progress curves were of similar shape and nonlineartime-courses of product formation were always observed. The results of kinetic modelling match the experimental data as indicated by the satisfying overlay of the experimental progress curves (dotted lines) with the curves obtained by kinetic modelling (solid lines). A more quantitative measure for the high quality of fitting constitutes the *B*-value (see Material and methods), which is significantly higher than 0.5 for all progress curves.

When the oxygenation rates measured at different oxygen concentrations (Fig. 2A) were plotted against the reaction time, a monotone decline of the rates was observed reaching steady-state kinetics after ≈100 s (Fig. 3). This time-dependent decline can be described by an exponential function containing as adjustable parameters the transition time $T_{0.5}$ (time at which the half-maximal rate was reached), the initial reaction rate v_{ini} and the steady-state rate v_{ss}. It should be noted, however, that additional experiments showed that the gradual decrease in the reaction rate was not due to suicidal enzyme inactivation (data not shown).

Initial rate kinetics of 15-LOX-catalysed 19-OH-AA oxygenation

To gain further insight into the kinetic peculiarities of 19-OH-AA oxygenation, the dependence of initial rates on substrate concentration was analysed. From Fig. 4A it can be seen that the dependence of the oxygenation rate on the concentration of 19-OH-AA can be described by the Michaelis–Menten equation yielding an apparent K_M of 90.0 μM (normoxic conditions). The corresponding value for arachidonic acid oxygenation under strictly comparable conditions was 10.3 μM (data not shown). These data are consistent with previous results on the oxygenation of hydroxylated fatty acid derivatives [20,21]. This significant difference in the K_M values is possibly due to the fact that introduction of a hydrophilic residue close to the methyl terminus of the fatty acid impairs substrate binding. It has been suggested before that burying a polar group in the hydrophobic environment of the substrate binding-pocket may be energetically hindered [20,22]. In Fig. 4B the dependence of the initial rates of 19-OH-AA oxygenation on the oxygen concentration is shown. It can be seen that even at oxygen concentrations as high as 800 μM, saturation conditions were not attained, a finding observed at two different concentrations of exogenous enzyme activator (13*S*-HpODE). These data are inconsistent with previous initial rate measurements of arachidonic acid oxygenation indicating oxygen K_M-values for various LOX-isoforms ranging between 10 and 20 μM [17]. Interestingly, the oxygen affinity of the enzyme/substrate complex was augmented at higher 13*S*-HpODE concentrations (Fig. 4B). These data suggest that the exogenous peroxide activator appears to impact the oxygen dependence of 19-OH-AA oxygenation. *Vice versa,* oxygen influenced the effectiveness of peroxide-dependent enzyme activation (Fig. 4C).

Consumption of 13S-HpODE during the time course of 19-OH-AA oxygenation

Since all progress curves had been monitored after preincubation of the enzyme with 13*S*-HpODE it was assumed that decomposition of the enzyme activator (13S-HpODE) might contribute to the time-dependent decay in reaction rates (Fig. 2) To test this hypothesis we incubated the 15-LOX under normoxic conditions

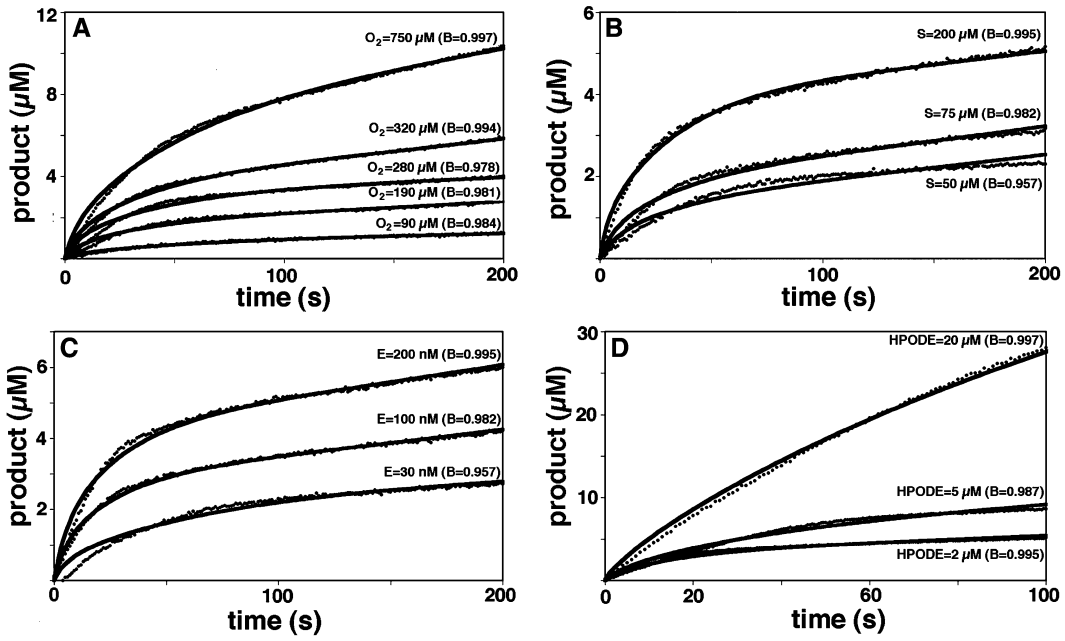

Fig. 2. Time courses of conjugated diene formation from 19-OH-AA at various initial experimental conditions. Kinetic progress curves (solid lines) were monitored spectrophotometrically as described in Experimental procedures. The solid lines represent the progress curved calculated with our kinetic model. The numbers in parenthesis indicate the quality of fitting of between the experimental and theoretical data (calculated using our complex kinetic model). *B*-values > 0.5 indicated high quality fitting. For the experiments shown in A, B and D the final enzyme concentration in the assay was 87 nM, for (A–C) the initial 13*S*-HpODE concentration was 1 μM. The maximal consumption of 19-OH-AA was < 10% of the initial concentration so that impact of substrate depletion on the shape of the time courses could be neglected. (A) Photometric progress curves of product formation at different oxygen concentrations (indicated at the traces). The concentration of 19-OH-AA was 200 μM. (B) Photometric progress curves of product formation at different concentrations of 19-OH-AA (indicated at the traces). The experiments were carried out under normoxic conditions (280 μM oxygen). (C) Photometric progress curves of product formation at different enzyme concentrations. Concentration of oxygen was 280 μM, concentration of 19-OH-AA was 200 μM. (D) Photometric progress curves of product formation at different activator concentrations (13S-HpODE). Concentration of oxygen was 280 μM, concentration of 19-OH-AA was 200 μM.

with 19-OH-AA in the presence of 4 μM 13*S*-HpODE and analysed the decay kinetics of the enzyme activator. From Fig. 5A it can be seen that, as expected, 13*S*-HpODE was decomposed during 19-OH-AA oxygenation. After 2 min almost 90% of the activator was already metabolized. These data indicate that the activator concentration gradually declined during the time course of reaction and this decline may contribute to the decrease in the enzymatic activity. However, this conclusion may only be valid if the product of 19-OH-AA oxygenation, the (5Z,8Z,11Z,13E,15S, 19S/R)-15-hydroperoxy-19-hydroxyeicosatetra-5,8,11,13-enoic acid (15-OOH-19OH-AA) is a less efficient LOX activator than 13S-HpODE. To confirm this hypothesis we prepared 13*S*-HpODE and 15-OOH-19OH-AA by HPLC and evaluated their capability to activate 15-LOX. Fig. 5B shows that 2 μM of 13S-HpODE was sufficient to completely abolish the kinetic lag-phase of arachidonic acid oxygenation (trace c). In contrast, 15-OOH-19OH-AA (trace b) was much less effective.

Conversion of 13S-HpODE to 13-keto-(9*Z*,11*E*)-octadecadienoic acid (13-KODE) during the time course of 19-OH-AA oxygenation

It has been reported previously that 13S-HpODE activates LOXs by converting the catalytically silent ferrous enzyme into an active ferric form [23]. This activation reaction is accompanied by conversion of 13*S*-HpODE. For the soybean LOX-1 it has been shown that ketodienes and superoxide ($O_2^{\cdot-}$) are formed during LOX–13S-HpODE interaction [24]. To test whether a similar reaction may proceed during rabbit 15-LOX-catalysed oxygenation of 19-OH-AA we monitored the absorbance at 275 nm during the time course of the reaction. From Fig. 6Aa it can be seen that there was a linear increase in absorbance at 275 nm and subsequent HPLC analysis indicated the formation of 13-KODE (Fig. 6B). In contrast, no conjugated ketodienes were formed when 19-OH-AA was omitted (Fig. 6Ab).

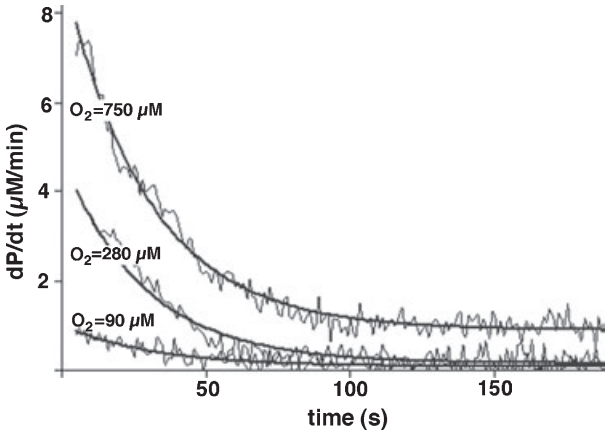

Fig. 3. Time courses of the rate of conjugated diene formation from 19-OH-AA. The thin oscillating traces represent the first derivative of the progress curve monitored at three different oxygen concentrations (Fig. 2A). The bold lines indicate the plot of the model function:

$$v(t) = [v_{ini} - v_{SS}]\exp\left(-\ln 2\frac{t}{T_{0.5}}\right) + v_{SS}$$

where v_{ini} and v_{ss} denote the initial rate and the steady-state rate, respectively. $T_{0.5}$ gives the half-time required for the time-dependent transition from the initial rate to the steady-state rate. The following parameters were estimated by fitting the model function to the experimental data by least-square minimization [O_2 (μm), v_{ini} (μm·min^{-1}), v_{ss} (μm·min^{-1}) and $T_{0.5}$ (s), respectively]: 550, 10.7, 0.92, 20; 280, 4.9, 0.18, 19; 90, 1.03, 0.11, 22.

Mechanistic considerations, kinetic modelling and general conclusions

Previous kinetic models of the LOX reaction did not consider oxygen dependence of enzyme activation [16,18,25]. To explain the mechanistic basis for the low oxygen affinity we tested various hypotheses: (a) as peroxide activation of the enzyme involves oxidation of the ferrous LOX to a ferric form we first considered the possibility of direct electron transfer from the ferrous nonheme iron to molecular dioxygen forming superoxide. However, such direct interaction is rather unlikely as there is no experimental evidence for oxygen binding at the ferrous nonheme iron [26]; (b) another potential explanation accounting for the observed synergistic effect of 13*S*-HpODE and oxygen during enzyme activation was to assume obstruction of oxygen penetration into the active site, which might be due to the presence of the polar hydroxyl group at C_{19}. Kinetic modelling of this scenario showed, however, that the enzyme/radical intermediate formed after hydrogen abstraction would accumulate leading to an enhanced inactivation of the enzyme and thus to a decrease of the initial rate with increasing concentrations of fatty acid substrate. Such a dependence is inconsistent with the observed increase in the initial rate with increasing substrate concentration (Fig. 4A).

Rejection of these direct explanations suggested an indirect effect of oxygen on LOX activation. It has been reported previously that molecular dioxygen is able to react with alkoxy radicals, which are formed during the reaction of the ferrous LOX with an activating hydroperoxy fatty acid [24]. Accordingly, we extended our previous kinetic model by three additional elementary reactions (Scheme 2): (a) Activation of the catalytically silent ferrous LOX is oxygen-dependent and involves the formation of ketodienes and superoxide. The initial step of peroxide dependent LOX activation [23,24] is a homolytic cleavage of the peroxy bond, which is paralleled by an electron transfer from the ferrous LOX to the hydroxy radical leaving an alkoxy radical and OH^-. This alkoxy radical may then reduce dioxygen to form superoxide and a stable keto-dienoic fatty acid. Alternatively, the alkoxy radical may stabilize via β-scission

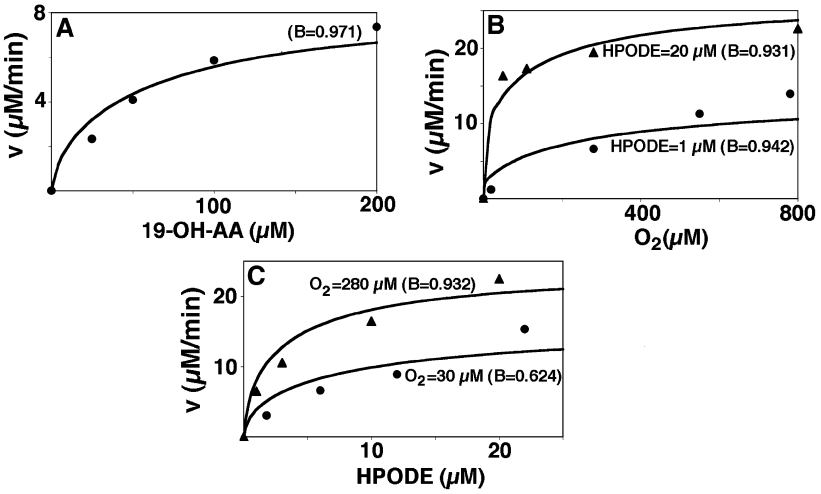

Fig. 4. Initial rates of 15-LOX catalysed oxygenation of 19-OH-AA under various experimental conditions. Initial rates were derived from the initial (linear) part of photometric progress curves and the symbols indicate the experimental data. (A) Initial rates at various concentrations of 19-OH-AA. (B) Initial rates at various oxygen concentrations. (C) Initial rates at various concentrations of 13*S*-HpODE.

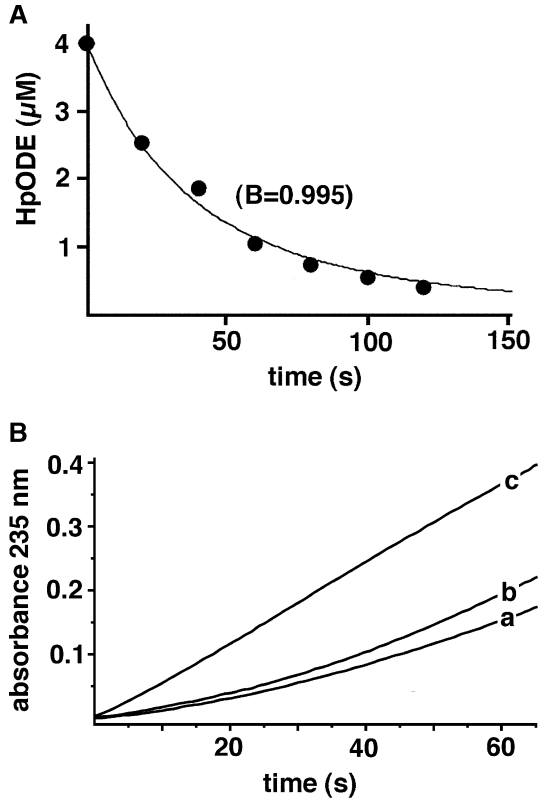

Fig. 5. Activation of ferrous LOX by 13S-HpODE and the oxygenation product of 19-OH-AA oxygenation. (A) Time course of 13*S*-HpODE decay during oxygenation of 19-OH-AA. The reaction was started at [19-OH-AA] = 100 μM, [O_2] = 280 μM, [HPODE] = 4 μM. The concentration of 13*S*-HpODE in the assay was determined by RP-HPLC at the time points indicated (filled circles). The solid line indicates the decay kinetics of 13*S*-HpODE calculated with our kinetic model. (B) Activating effect of 13*S*-HpODE and 15-OOH-19-OH-AA on the oxygenation rate of arachidonic acid in the absence of activating peroxide. Photometric progress curves were monitored at normoxic conditions. Trace (a) no activator, trace (b) 2 μM 15-OOH-19-OH-AA as activator, trace (c) 2 μM 13*S*-HpODE as activator.

of the hydrocarbon chain, via epoxidation or dimerization [24]. (b) Escape of the catalytically inactive ferrous LOX from the catalytic cycle. When the catalytically active ferric LOX catalyses hydrogen abstraction a LOX/fatty acid radical complex (E^{2+}–S$^{\cdot}$) is formed. Insertion of molecular dioxygen subsequently yields a LOX/fatty acid hydroperoxy radical complex (E^{2+}–SOO$^{\cdot}$). Both catalytic intermediates contain the enzyme in its catalytically silent ferrous form. When these complexes decay inactive enzyme escape the catalytic cycle and thus, requires additional activation to re-enter again. Leakage of the ferrous enzyme from the oxygenation cycle is paralleled by release of radical intermediates (either S$^{\cdot}$ or SOO$^{\cdot}$). Nonenzymatic reaction of S$^{\cdot}$ with molecular dioxygen should be indicated by a portion of stereo-random oxygenation products. However, we never observed a significant formation of stereo-random oxygenation products despite specifically looking for it. Leakage of SOO$^{\cdot}$ from the catalytic cycle may not alter the stereospecific product pattern and thus, in the light of our inability to detect stereo-random oxygenation products, decay of the E^{2+}–SOO$^{\cdot}$-complex was more likely. (c) Radical recombination at the active site. The superoxide anion (O_2^-) formed during the activation reaction may recombine with the E^{2+}–S$^{\cdot}$-complex. Thus, our amended kinetic model does also consider the possibility of a direct interaction of superoxide with the LOX/fatty acid radical complex.

Derivation of the kinetic equations governing the reaction scheme is described in Experimental procedures. Numerical values for the rate constants and binding parameters were obtained by fitting the kinetic model to the experimental data. The calculated parameter values are summarized in Table 2. Taken together one may conclude that our kinetic model provides a satisfying quantitative description of our experimental data. It has to be admitted, however, that the model provides a poor fit to the initial-rate data in cases where either concentration of oxygen is very high and concentration of HpODE is low (lower curve in Fig. 4B) or vice versa (lower curve in Fig. 4C). We have to conclude that the true kinetics of the interaction of these metabolites with the enzyme and their interplay in the activation process is not fully covered by our model. It is thinkable, for example, that HpODE at sufficiently high concentrations is capable of reacting with both the ferric and ferryl iron as shown for its reaction with myoglobin [27].

Several mechanistic conclusions, which can be deduced from the model, are highlighted below.

(a) Consistent with our experimental results the model predicts a biphasic dependence of the reaction rate on oxygen concentration (high and a low affinity component of oxygen uptake). The nonsaturable low-affinity component may be attributed to oxygen consumption associated with re-activation of the catalytically silent ferrous LOX that is permanently formed predominantly *via* decay of the enzyme/peroxy radical complex (E^{2+}–SOO$^{\cdot}$). This conclusion is supported by an additional step of *in silico* modelling. If one plots the initial rates of 19-OH-AA oxygenation vs. oxygen concentrations at various values of the rate constant k^*_{PO} [reaction step (E^{2+}–SOO$^{\cdot}$) → (SOO$^{\cdot}$) + (E^{2+})] the curves shown in Fig. 4 are obtained. If one reduces k^*_{PO} by two orders of magnitude the low-affinity component of the oxygen uptake

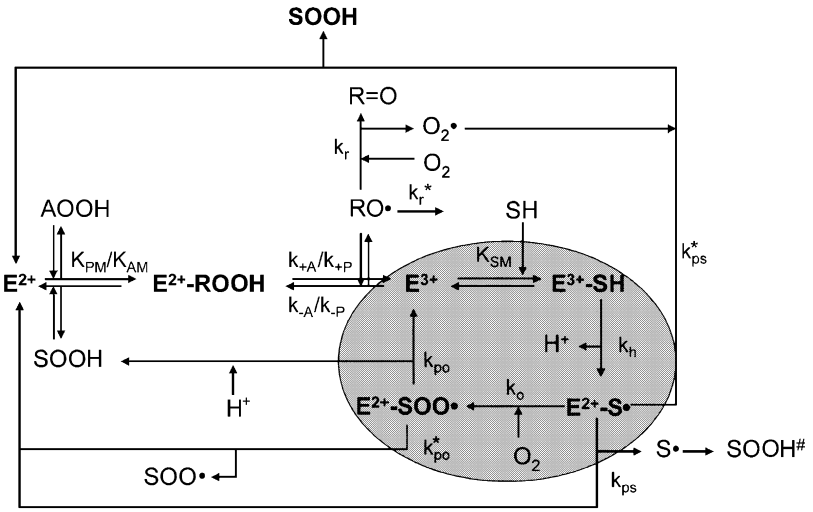

Scheme 2. Reaction scheme for lipoxygenases. The catalytically silent ferrous LOX (E^{2+}) is activated to an ferric form (E^{3+}) reacting either with the reaction product of 19-OH-AA oxygenation (19-OH,15-OOH-AA; SOOH in Scheme 2, binding constant K_{PM}) or with an exogenous activator (13S-HpODE, AOOH in Scheme 2, binding constant K_{AM}). ROOH symbolizes either SOOH (substrate hydroperoxide) or AOOH (exogenous activator hydroperoxide). Overall, the activation process involves homolytic cleavage of the peroxy bond of the activating hydroperoxide (ROOH, which can be SOOH or AOOH) and reduction of molecular dioxygen forming superoxide [24]. The alkoxy radical (RO•) may react with dioxygen to form a keto dienoic fatty acid (k_r) and superoxide. Alternatively, RO• may stabilize *via* the formation of β-scission or epoxidation products (k^*_r). The oxygenation cycle (highlighted in grey) starts with substrate binding at the active site of the ferric enzyme (K_{SM}) followed by hydrogen abstraction from a bisallylic methylene (k_h). With naturally occurring fatty acid as substrates hydrogen abstraction is rate limiting and releases a proton. The corresponding electron is transferred to the ferric nonheme iron reducing it back to a ferrous form. The resulting enzyme/substrate radical complex (E^{2+}–S•) may react with molecular dioxygen (k_O) to form the enzyme/peroxy radical complex (E^{2+}–SOO•). In addition, there are two other option for the reaction of E^{2+}–S•. It may decay (k_{PS}) liberating the inactive ferrous enzyme (E^{2+}) and the substrate radical (S•), which may subsequently undergo conversion to stereo-random oxygenation products (SOOH•). Alternatively, enzyme-bound S• may be retained at the active site and may recombine with superoxide (k^*_{PS}) to form stereospecific hydroperoxy product (SOOH). The ferrous enzyme/substrate peroxy radical complex (E^{2+}–SOO•) is stabilized during the catalytic cycle via intracomplex electron transfer, which reduces the substrate peroxy radical to the corresponding anion and oxidizes the enzyme back to the catalytically active ferric form (E^{3+}). Alternatively, the E^{2+}–SOO• may decay (k^*_{PO}) releasing a peroxyl radical (SOO•). Binding of the fatty acid substrate (SH) to the active (ferric) enzyme (catalytic cycle) and of the hydroperoxy compounds (either AOOH or SOOH) to the inactive (ferrous) enzyme (activation reaction) is described as rapid equilibrium characterized by the Michaelis constants K_{SM} and K_{PM}/K_{AM}, respectively.

(slope of the curve at high oxygen concentration; see Fig. 7) did almost disappear. In fact, under such condition the oxygen dependence is reduced to a hyperbolic curve with a Michaelis constant in the range between 5 and 10 μM. Such curves are typical for naturally occurring polyenoic fatty acids (arachidonic acid, linoleic acid). Remarkably, the simulated curves in Fig. 7 indicate an increase in the reaction rate with decreasing values for k^*_{PO}. This can be explained by the fact that a frequent dropout of the enzyme from the catalytic cycle as suggested for 19-OH-AA oxygenation may be one reason for the low oxygenation rates of this substrate.

(b) The kinetic model predicts two possibilities for reversible enzyme inactivation (decay of E^{2+}–S•- and E^{2+}–SOO•-complexes). E^{2+}–SOO• decays with the rate constant $k^*_{PO} = 2.2\ s^{-1}$ whereas E^{2+}–S• decays much slower ($k_{PS} = 0.0009\ s^{-1}$) and thus may not be relevant. Our inability to detected stereo-random oxygenation products even under experimental conditions at which decay of E^{2+}–S• was expected to be favoured is consistent with this conclusion. Intriguingly, our modelling results point to predominant reversible inactivation of the enzyme via decay of the complex E^{2+}–SOO• with hydroxylated arachidonic acid as substrate, whereas reversible inactivation of the enzyme with arachidonic acid as substrate has been reported to proceed predominantly *via* decay of E^{2+}–S•-complex whereby the values of the decay constant (k_{PS}) varied between $1\ s^{-1}$ [28] and $300\ s^{-1}$ [25].

(c) The rate constant k_{+A} for 13*S*-HpODE-dependent enzyme activation is about twofold higher than the corresponding value (k_{+P}) determined for the product of 19-OH-AA oxygenation (15-OOH-19-OH-AA). Moreover, the Michaelis constants for binding of 13*S*-HpODE (K_{AM}) and 15-OOH-19-OH-AA (K_{PM}) to the ferrous enzyme (E^{2+}) also differ by a factor of

Table 2. Numeric values of the kinetic constants in reaction Scheme 2.

Model parameter	Meaning	Estimated value	Variation of parameter value providing not more than 5% increase of residual square sum
k_{+A}	Enzyme activation ($E^{2+} \rightarrow E^{3+}$) by AOOH (13*S*-HpODE)	12.8 $s^{-1}\cdot\mu M^{-1}$	0.97 $s^{-1}\cdot\mu M^{-1}$
k_{-A}	Enzyme inactivation ($E^{3+} \rightarrow E^{2+}$) by AO$^{\cdot}$ (formed from 13*S*-HpODE)	122.2 $s^{-1}\cdot\mu M^{-1}$	12.2 $s^{-1}\cdot\mu M^{-1}$
k_{+P}	Enzyme activation ($E^{2+} \rightarrow E^{3+}$) by SOOH (19-OH,15OOH-AA)	7.0 $s^{-1}\cdot\mu M^{-1}$	0.4 $s^{-1}\cdot\mu M^{-1}$
k_{-P}	Enzyme inactivation ($E^{3+} \rightarrow E^{2+}$) by SO$^{\cdot}$ (formed from19-OH,15OOH-AA)	8.5 $s^{-1}\cdot\mu M^{-1}$	0.8 $s^{-1}\cdot\mu M^{-1}$
k_h	Hydrogen abstraction	10.1 s^{-1}	0.5 s^{-1}
k_o	Oxygen insertion	1.6 $s^{-1}\cdot\mu M^{-1}$	0.08 $s^{-1}\cdot\mu M^{-1}$
k_{PO}	Product formation (intracomplex electron transfer)	28.3 s^{-1}	2.8 s^{-1}
k^*_{PO}	Decay of E^{2+}–SOO$^{\cdot}$-complex	2.2 s^{-1}	0.2 s^{-1}
k_{PS}	Decay of E^{2+}–S$^{\cdot}$-complex	0.0009 s^{-1}	0.00005 s^{-1}
k^*_{PS}	Reaction of the E^{2+}–S$^{\cdot}$-complex with superoxide ($O_2^{-\cdot}$)	1222 $s^{-1}\cdot\mu M^{-1}$	60.9 $s^{-1}\cdot\mu M^{-1}$
k_r	Reaction of the alkoxy radical RO$^{\cdot}$ (AO$^{\cdot}$ or SO$^{\cdot}$) with superoxide ($O_2^{-\cdot}$)	0.0024 $s^{-1}\cdot\mu M^{-1}$	0.00025 $s^{-1}\cdot\mu M^{-1}$
k^*_r	Oxygen independent conversion of the alkoxy radical RO$^{\cdot}$	0.032 s^{-1}	0.0022 s^{-1}
K_{SM}	Binding of substrate (19-OH-AA) to the ferric enzyme	77.26 μM	3.86 μM
K_{PM}	Binding of product (19-OH,15-OOH-AA) to the ferrous enzyme	104.9 μM	5.2 μM
K_{AM}	Binding of activator (13*S*-HpODE) to the ferrous enzyme	31.2 μM	2.3 μM

three. Thus, according to our modelling the enzyme is less effectively activated by 15-OOH-19-OH-AA (endogenous activator) when compared with 13*S*-HpODE (exogenous activator). These inferences from the model are consistent with the experimental findings shown in Fig. 5B.

(d) Under normoxic conditions the value for the apparent first-order rate constant of the oxygen-dependent conversion of the alcoxyl radical into keto-dienes amounts to $k_r \times 280\ \mu M = 0.67\ s^1$. This value is much larger than that of the rate constant $k^*_r = 0.032\ s^{-1}$ for oxygen-independent conversion of the alkoxy radical. Thus, oxygen independent rearrangement of the alkoxy radical appears to be negligible for 19-OH-AA oxygenation.

Taken together, the proposed kinetic model (Scheme 2) provides a satisfactory quantitative description of all experimental data obtained in this study. The major mechanistic consequence of our model is that oxygen exhibits a dual role during the lipoxygenase reactions. It serves as a substrate but also constitutes an enzyme activator. The latter function has never been described before because it can hardly be detected with naturally occurring polyenoic fatty acids. The biological importance of LOXs is commonly discussed in relation to the synthesis of bioactive mediators involved in inflammation, metastasis or osteoporosis [4,8,11]. Additionally, these enzymes have been implicated in structural alterations of complex lipid–protein assemblies, such as biomembranes and lipoproteins, impacting on cell maturation and atherogenesis [6,7,9,10]. Here we report that, under certain conditions, the LOX reaction may serve as a source of free radicals ($O_2^{-\cdot}$, S$^{\cdot}$, or SOO$^{\cdot}$) and that release of these reaction intermediates may increase the multiplicity of LOX-induced secondary reactions. Under normal conditions (normoxia, free fatty acids as substrate) the LOX reaction may not be considered an effective radical source a all radical intermediates remain enzyme bound. However, with more complex substrates, under hypoxic conditions and after pH variations, free radicals may escape the catalytic cycle and then induce secondary co-oxidations [15,16]. Such co-oxidation reactions have actually been implicated in oxidative metabolism of xenobiotics, including drugs [29].

Experimental procedures

Chemicals

The chemicals used were from the following commercial sources: (5Z,8Z,11Z,14Z)-eicosa-5,8,11,14-tetraenoic acid (arachidonic acid), (9Z,12Z)-octadeca-9,12-dienoic acid (linoleic acid) and sodium borohydride from Serva (Heidelberg, Germany); *N*-nitroso-*N*-methylurea and bis(trimethylsilyl)trifluoroacetamide (BSTFA) from Sigma (Deisenhofen, Germany), sodium dithionite, NADH and 10% Pd/$CaCO_3$ (catalyst for hydrogenation) from Aldrich (Taufkirchen, Germany); HPLC solvents from Merck (Darmstadt, Germany). (19*R/S*,5Z,8Z,11Z,14Z)-19-hydroxyeicosa-5,8,

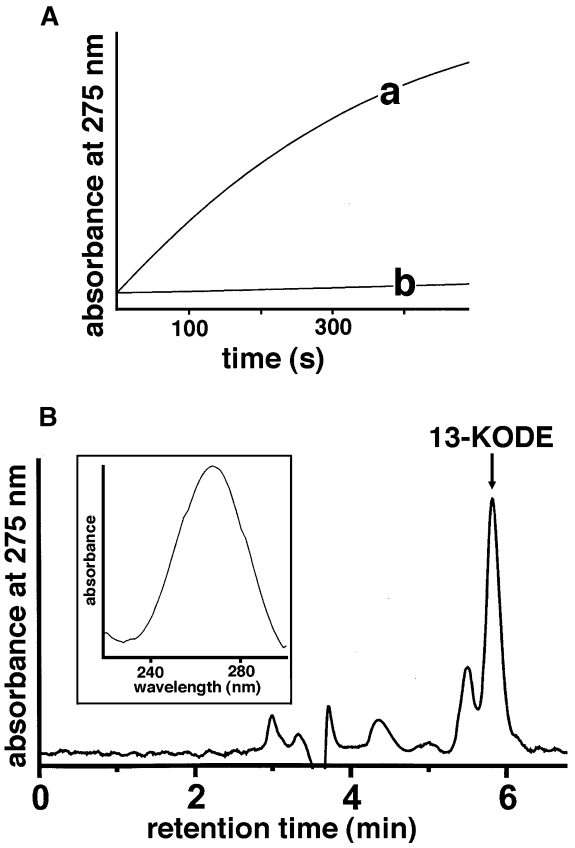

Fig. 6. Formation of ketodienes during 15-LOX catalysed oxygenation of 19-OH-AA. (A) 15-LOX was incubated in with 19-OH-AA (87 nM enzyme, 200 μM 19-OH-AA, 40 μM 13S-HpODE, 280 μM oxygen) and the increase in absorbance at 275 nm was recorded (a, complete sample; b, no19-OH-AA). (B) After 10 min the reaction was terminated by the addition of an equal volume of methanol, lipids were extracted, purified by RP-HPLC and further analysed by SP-HPLC using the solvent system n-hexane:2-propanol:acetic acid (100 : 2 : 01, v/v/v). The retention time of an authentic standard of 13-KODE is given above the trace. Inset: uv-spectrum of the peak coeluted with the authentic standard of 13-KODE indicating a conjugated ketodiene chromophore.

11,14-tetraenoic acid (19-OH-AA) was synthesized for this study in a similar way as described in [30]. The chemical structures of arachidonic acid and 19-OH arachidonic acid are shown in Fig. 1.

Enzyme preparation

The rabbit 15-LOX [31] was prepared from a stroma-free supernatant of a reticulocyte-rich blood cell suspension by sequential fractionated ammonium sulfate precipitation, hydrophobic interaction chromatography (Phenyl-5-PU column, Biorad, Munich, Germany) and anion exchange chromatography (Resource Q column, Amersham Bioscience, Freiburg, Germany). The final enzyme preparation was

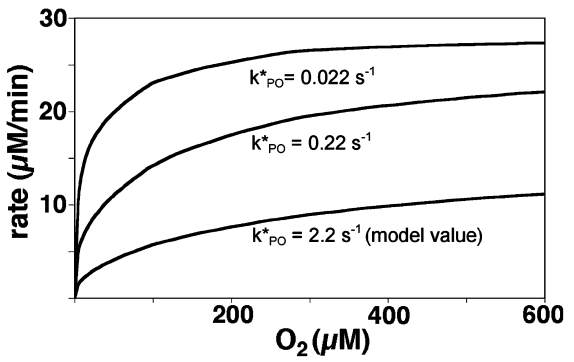

Fig. 7. Predicted oxygen dependence of the initial reaction rate of 19-OH-AA oxygenation at various values of the rate constant k_{PO}* (decay of Fe^{2+}–$SOO^{\cdot}$-complex). According to our kinetic model the decay of the Fe^{2+}–$SOO^{\cdot}$-complex, which leads to release of the peroxy radical ($SOO^{\cdot}$), constitutes the major reason for reversible enzyme inactivation. Initial rates were computed on the basis of the kinetic model using the numerical values of the parameters listed in Table 2.

> 95% pure (see supplement) and its molecular turnover rate of linoleic acid was 25 s^{-1}. The enzyme exhibited a dual positional specificity with arachidonic acid (12-HpETE/15-HpETE ratio of 1 : 9) and converted linoleic acid exclusively to 13S-HpETE.

Kinetic assays

The LOX reaction was followed either spectrophotometrically by measuring the increase in absorbance at 234 nm, or oxygraphically using a Clark-type oxygen electrode. For photometric measurements a Shimadzu UV2100 spectrophotometer was used. The reaction mixture was 0.1 M potassium phosphate buffer pH 7.4, containing variable concentrations of substrate fatty acids and/or oxygen (total assay volume 1 mL). The enzyme was preincubated in the assay buffer for ≈10 s and then the reaction was started by addition of a small aliquot (5–10 μL) of a substrate solution. To avoid kinetic lag periods and extensive suicidal inactivation the assay sample was supplemented with 1 μM 13S-HpODE and the reaction was carried out at 20 °C. Various oxygen concentrations were adjusted by mixing aliquots of oxygen-free reaction buffer (repeated evacuation and flushing with argon gas) with oxygen saturated reaction mixtures. For the oxygraphic measurements a Strathkelvin oxygen meter 781 (Strathkelvin Instruments, Glasgow, UK) was used. Sample composition was the same as for the spectrophotometric measurements but the reaction volume was reduced to 0.4 mL. The oxygraphic scale was calibrated by repeated injection of known amounts of NADH to a mixture of submitochondrial particles.

Kinetic modelling

For the derivation of the rate equations it was assumed that for the concentrations of the reactants used in the experiments, binding of the fatty acid substrate to the ferrous enzyme and binding of the hydroperoxy fatty acids (reaction product or exogenous activator) to the ferric enzyme could be neglected. Treating the binding of fatty acid substrate (S) to the ferric enzyme and the binding of the peroxide activator (SOOH or AOOH) to the enzyme as fast reversible equilibrium reactions one may introduce the enzyme pools:

$$\begin{aligned} X_1 &= [E^{2+}] + [E^{2+}{-}AOOH] + [E^{2+}{-}SOOH] \\ X_2 &= [E^{3+}] + [E^{3+}{-}S] \\ X_3 &= [ES^{\cdot}] \\ X_4 &= [ESOO^{\cdot}], \end{aligned} \tag{1}$$

which add up to the total enzyme

$$E_0 = X_1 + X_2 + X_3 + X_4.$$

The kinetic equations governing the time-dependent concentration changes of the reactants and enzyme pools read:

$$\begin{aligned} \frac{d(S)}{dt} &= -f_2(X_2) \\ \frac{d(O_2)}{dt} &= -f_4(X_3) - k_r(O_2)[(SO^{\cdot}) + (AO^{\cdot})] \\ \frac{d(SOOH)}{dt} &= [f_5 + f_6](X_4) + f_3(X_3) - f_{1P}(X_1) + f_{-1P}(X_2) \\ \frac{d(AOOH)}{dt} &= -f_{1A}(X_1) + f_{-1A}(X_2) \\ \frac{d(SO^{\cdot})}{dt} &= f_{1P}(X_1) - [f_{-1P}(X_2) + k_r(O_2) + k_r^*](SO^{\cdot}) \\ \frac{d(AO^{\cdot})}{dt} &= f_{1A}(X_1) - [f_{-1A}(X_2) + k_r(O_2) + k_r^*](AO^{\cdot}) \\ \frac{d(O_2^{-})}{dt} &= k_r(O_2)[(SO^{\cdot}) + (AO^{\cdot})] - k_{PS}^*(O_2^{\cdot})(X_2) \end{aligned} \tag{2}$$

and

$$\begin{aligned} \frac{d(X_1)}{dt} &= f_3(X_3) + f_6(X_4) - [f_{1P} + f_{1A}](X_1) + [f_{-1P} + f_{-1A}](X_2) \\ \frac{d(X_2)}{dt} &= [f_{1P} + f_{1A}](X_1) - [f_{-1P} + f_{-1A}](X_2) + f_5(X_4) - f_2(X_2) \\ \frac{d(X_3)}{dt} &= f_2(X_2) - [f_3 + f_4](X_3) \\ \frac{d(X_4)}{dt} &= f_4(X_3) - [f_5 + f_6](X_4) \end{aligned} \tag{3}$$

In Eqn (2), the variables $(SO^{\cdot})$ and $(AO^{\cdot})$ denote the alkoxyl radicals resulting from the homolytic cleavage of the peroxy bond in the product of 19-OH-AA oxygenation (=SOOH in Scheme 2) and in 13*S*-HpODE (=AOOH in Scheme 2), which act as exogenous enzyme activators.

The rate functions f_{1P}, f_{1H}, f_{-1P}, f_{-1H}, f_2, f_3, f_4, f_5, f_6 and f_7 appearing in the equation systems (2) and (3) are defined as follows:

$$\begin{aligned} f_{1P} &= \frac{k_{+P}(SOOH)}{K_{PM}(1 + (AOOH)/K_{AM}) + (SOOH)} \\ f_{1A} &= \frac{k_{+A}(AOOH)}{K_{AM}(1 + (SOOH)/K_{PM}) + (AOOH)} \\ f_{-1P} &= \frac{k_{-P}(SO^{\cdot})}{1 + (S)/K_{SM}} \\ f_{-1A} &= \frac{k_{-A}(AO^{\cdot})}{1 + (S)/K_{SM}} \\ f_2 &= \frac{k_h(S)}{K_{SM} + S} \\ f_3 &= k_{PS} + k_{PS}^*(O_2^{\cdot}) \\ f_4 &= k_O(O_2) \\ f_5 &= k_{PO} \\ f_6 &= k_{PO}^* \end{aligned} \tag{4}$$

Here K_{PM} and K_{AM} denote the dissociation constant for binding of the enzymatically formed product and the activator HpODE to the ferrous enzyme and K_{SM} is the dissociation constant for bonding of the fatty acid substrate to the ferric enzyme.

The kinetic Eqns (2–4) have been set up by expressing the concentration of pool variables through mass-action relations and by applying the rules of chemical reaction kinetics to the total pools, i.e. the time-dependent variation of a model variable is positively affected by any elementary process forming the variable and negatively affected by any elementary process degrading the variable. For example, the concentration of dioxygen (O_2) can only be diminished during the lipoxygenase reaction namely by the following three processes: (a) reaction with the enzyme–radical-complex (E^{2+}–$S^{\cdot}$) which represents a bi-molecular reaction possessing the rate $k_o(O_2)$ (E^{2+}–$S^{\cdot}$); (b) reaction with the product-derived alcoxy radical ($SO^{\cdot}$) generated during enzyme activation through the reaction product; this is also a bi-molecular reaction possessing the rate $k_r(O_2)$ ($SO^{\cdot}$); or (c) reaction with the activator-derived alcoxy radical ($AO^{\cdot}$). The rates of these three processes appear at the right-hand side of the second differential equation in Eqn (2) describing the time-dependent variation of dioxygen.

Note that in the definition of the rate functions Eqn (4) the assumption was made that under assay conditions the concentration of the alkoxy radicals remains much smaller than the corresponding dissociation constants for the formation of the enzyme–radical-complex. Within a short time interval determined by the smallest rate function among f_{1P}, f_{1A}, f_{-1P}, f_{-1A}, f_2, f_3, f_4, f_5, f_6, k_r, k_r* a quasi-equilibrium state is established where the time-derivatives of the enzyme pools (X_i) and of the intermediates ($SO^{\cdot}$) and ($AO^{\cdot}$) can be put to zero:

$$\frac{d(X_i)}{dt} = 0 \qquad (i = 1, 2, 3, 4) \tag{5.1}$$

$$\frac{d(SO^{\cdot})}{dt} = \frac{d(AO^{\cdot})}{dt} = 0 \quad (5.2)$$

Solution of the algebraic system (5.1) yields:

$$(X_i) = C_i(X)/(C_1 + C_2 + C_3 + C_4) \quad (6)$$

with

$$\begin{aligned}(C_1) &= \{[f_{-1P}(SO^{\cdot}) + f_{-1A}(AO^{\cdot})][f_3 + f_4] + [f_2 f_3]\} \\ &\quad \times [f_5 + f_6] + f_2 f_4 f_6 \\ (C_2) &= (f_{1P} + f_{1A})(f_3 + f_4)(f_5 + f_6) \\ (C_3) &= (f_{1P} + f_{1A}) f_2 (f_5 + f6) \\ (C_4) &= (f_{1P} + f_{1A}) f_2 f_4\end{aligned} \quad (7)$$

Under quasi steady-state conditions expressed by Eqns (5.1–5.2) the last two equations of system (7) can be rewritten as:

$$\begin{aligned}(SO^{\cdot}) &= \frac{f_{1P}(X_1)}{f_{-1P}(X_2) + k_r(O_2) + k_r^*} \\ (AO^{\cdot}) &= \frac{f_{1A}(X_1)}{f_{-1A}(X_2) + k_r(O_2) + k_r^*}\end{aligned} \quad (8)$$

Eqn (8) are self-consistent equations of the type $y = f(y)$ with respect to the variables SO and AO because the variable C_1 and thus the pool variables X_1 and X_2 depend on (SO) and (AO) according to the definitions in Eqn (6). Eqn system (8) was solved by means of an iterative solution method, $y_n = f(y_{n-1})$, $n = 1,2,\ldots$ The kinetic equations governing the time-dependent variation of the fatty acid substrate, oxygen, hydroperoxy product and 13*S*-HpODE finally read:

$$\begin{aligned}\frac{d(S)}{dt} &= -v_S \\ \frac{d(O_2)}{dt} &= -v_O \\ \frac{d(SOOH)}{dt} &= v_P \\ \frac{d(AOOH)}{dt} &= -v_H \\ \frac{d(O_2^{\cdot})}{dt} &= v_{OR}\end{aligned} \quad (9)$$

where the steady-state rate equations v_O, v_S, v_P, v_H and v_{or} are defined as follows:

$$\begin{aligned}v_O &= f_4(X_3) + k_r(O_2)[(SO^{\cdot}) + (AO^{\cdot})] \\ v_S &= f_2(X_2) \\ v_P &= (f_5 + f_6)(X_4) - f_{1P}(X_1) + f_{-1P}(X_2) \\ v_H &= -f_{1A}(X_1) + f_{-1A}(X_2) \\ v_{OR} &= k_r[(AO^{\cdot}) + (SO^{\cdot})](O_2) - k_{PS}^*(X_3)(O_2^{\cdot})\end{aligned} \quad (10)$$

Note that the concentration of the alcoxy radicals (SO) and (AO) appearing in the rate Eqns (10) are to be calculated from the self-consistent Eqns (8) by means of an iteration procedure. The initial rates are given by the rate Eqns (10) with $(P) = (O_2) = 0$.

Data smoothing and calculation of initial rates

To improve the signal/noisebratio for the calculation of the first derivatives (reaction rates), progress curves obtained by oxygraphic measurements were smoothed using a sliding average procedure. For any time point of the progress curve, the value of the variable monitored was calculated as the arithmetic mean taken over the values of the 10 preceeding and 10 succeeding data points. Initial reaction rates were calculated from the slope of the initial part of the spectrophotometric progress curves.

Statistical evaluations

The quality of fitting of the kinetic model to the various sets of experimental data was determined by the *coefficient of determination* B being the ratio of the explained variation of the data to the total variation. For linear regression models, the coefficient of determination is the squared value of the regression coefficient r, i.e. $B = r^2$. For arbitrary (nonlinear) models $y^{model} = f(x)$ the coefficient of determination can be defined by:

$$B = 1 - \frac{\sum_i \left[y_i^{exp} - y_i^{model}\right]^2}{\sum_i \left[y_i^{exp} - \hat{y}\right]^2} \quad (11)$$

where the numerator of the quotient in Eqn (11) represents the sum of deviation squares between the observed and calculated data points and the denominator represents (up to a scaling factor) the variance of the observed data [32]. The *coefficient of determination* represents the percent of the data that is the closest to the curve of best fit. For example, if $B = 0.850$, it means that 85% of the total variation in y can be explained by the modelled relationship between x and y. The other 15% of the total variation in y remains unexplained.

Fitting procedure

Fitting of the kinetic model to the experimental data was performed by using a Visual Basic program that combines solution of the differential equation system (9–10) by means of a fifth order Runge–Kutta integration procedure with a nonlinear regression method (Frontline Solver 5.5, Frontline Systems Inc. USA).

Construction of error bounds on the kinetic parameters

To indicate how well the numerical model parameters were determined by the experimental data a confidence interval for each parameter was determined. For this purpose the parameters were either increased or decreased in small steps (1% alteration in each step) until the value of the total sum of least squares for either the progress curve data or the ini-

tial rate data had increased by 5%. This procedure yielded an interval for the corresponding parameter in which the difference between the theoretical curve and experimental data did not exceed 5%. The confidence interval was set to 50% of this interval, i.e. $(p_u–p_l)/2$ with p_u and p_l denoting the upper and lower boundary.

This paper was supported in part by the European Commission (FP6, LSHM-CT-0050333). The Commission is not liable for any use that may be made of the information herein.

References

1 Kuhn H & Thiele B (1999) The diversity of the lipoxygenase family. Many sequence data but little information on biological significance. *FEBS Lett* **449**, 7–11.
2 Brash AR (1999) Lipoxygenases: occurrence, functions, catalysis, and acquisition of substrate. *J Biol Chem* **274**, 23679–23682.
3 Feussner I & Wasternack C (2002) The lipoxygenase pathway. *Annu Rev Plant Biol* **53**, 275–297.
4 Funk CD (2001) Prostaglandins and leukotrienes: Advances in Eicosanoid biology. *Science* **294**, 1871–1875.
5 Aliberti J, Hieny S, Reis-e, -Sousa C, Serhan CN & Sher A (2002) Lipoxin-mediated inhibition of IL-12 production by DCs: a mechanism for regulation of microbial immunity. *Nat Immunol* **3**, 76–82.
6 Rapoport SM, Schewe T & Thiele B (1990) Maturational breakdown of mitochondria and other organelles in reticulocytes. *Blood Cell Biochem* **1**, 151–194.
7 van Leyen K, Duvoisin RM, Engelhardt H & Wiedmann M (1998) A function for lipoxygenase in programmed organelle degradation. *Nature* **395**, 392–395.
8 Pidgeon GP, Kandouz M, Meram A & Honn KV (2002) Mechanisms controlling cell cycle arrest and induction of apoptosis after 12-lipoxygenase inhibition in prostate cancer cells. *Cancer Res* **62**, 2721–2727.
9 Cyrus T, Witztum JL, Rader DJ, Tangirala R, Fazio S, Linton MRF & Funk CD (1999) Disruption of the 12/15-lipoxygenase gene diminishes atherosclerosis in apo E-deficient mice. *J Clin Invest* **103**, 1597–1604.
10 Cathcart MK & Folcik VA (2000) Lipoxygenases and atherosclerosis: protection versus pathogenesis. *Free Rad Biol Med* **28**, 1726–1734.
11 Klein RF, Allard J, Avnur Z, Nikolcheva T, Rotstein D, Carlos AS, Shea M, Waters RV, Belknap JK, Peltz G & Orwoll ES (2004) Regulation of bone mass in mice by the lipoxygenase gene Alox15. *Science* **303**, 229–232.
12 Drazen JM, Israel E & O'Byrne PM (1999) Treatment of asthma with drugs modifying the leukotriene pathway. *N Engl J Med* **340**, 197–206.
13 Wenzel SE & Kamada AK (1996) Zileuton: the first 5-lipoxygenase inhibitor for the treatment of asthma. *Ann Pharmacother* **30**, 858–864.
14 Nelson MJ, Cowling RA & Seitz SP (1994) Structural characterization of alkyl and peroxyl radicals in solutions of purple lipoxygenase. *Biochemistry* **33**, 4966–4973.
15 Noguchi N, Yamashita H, Hamahara J, Nakamury A, Kühn H & Niki E (2002) The specificity of lipoxygenase-catalyzed lipid peroxidation and the effects of radical scavenging antioxidants. *Biol Chem* **383**, 619–626.
16 Berry H, Débat H & Larreta-Garde V (1998) Oxygen concentration determines regiospecificity in soybean lipoxygenase-1 reaction via a branched kinetic scheme. *J Biol Chem* **273**, 2769–2776.
17 Juranek I, Suzuki H & Yamamoto S (1999) Affinities of various mammalian arachidonate lipoxygenases and cyclooxygenases for molecular oxygen as substrate. *Biochim Biophys Acta* **1436**, 509–158.
18 Ludwig P, Holzhütter HG, Colosimo A, Silvestrini Ch, Schewe T & Rapoport SM (1987) A kinetic model for lipoxygenases based on experimental data with the lipoxygenase of reticulocytes. *Eur J Biochem* **168**, 325–337.
19 Ruddat VC, Whitman S, Holman TR & Bernasconi CF (2003) Stopped-flow kinetic investigations of the activation of soybean lipoxygenase-1 and the influence of inhibitors on the allosteric site. *Biochemistry* **42**, 4172–4178.
20 Ivanov I, Schwarz K, Holzhütter HG, Myagkova G & Kühn H (1998) Soybean lipoxygenase-1 oxygenates synthetic polyenoic fatty acids with an altered positional specificity: evidence for inverse substrate alignment. *Biochem J* **336**, 345–352.
21 van-Os CP, Rijke-Schilder GP, van Halbeek H, Verhagen J & Vliegenthart JF (1981) Double dioxygenation of arachidonic acid by soybean lipoxygenase-1. Kinetics and regio-stereo specificities of the reaction steps. *Biochim Biophys Acta* **663**, 177–193.
22 Browner M, Gillmor SA & Fletterick R (1998) Burying a Charge. *Nat Struct Biol* **5**, 179.
23 de Groot JJ, Garssen GJ, Veldink GA, Vliegenthart JF & Boldingh J (1975) On the interaction of soybean lipoxygenase-1 and 13-L-hydroperoxylinoleic acid, involving yellow and purple coloured enzyme species. *FEBS Lett* **56**, 50–54.
24 Chamulitrat W, Hughes MF, Eling TE & Mason RP (1991) Superoxide and peroxyl radical generation from the reduction of polyunsaturated fatty acid hydroperoxides by soybean lipoxygenase. *Arch Biochem Biophys* **1**, 153–159.
25 Schilstra MJ, Veldink GA & Vliegenthart JF (1994) The dioxygenation rate in lipoxygenase catalysis is determined by the amount of iron (III) lipoxygenase in solution. *Biochemistry* **33**, 3974–3979.
26 Glickman MH & Klinman JP (1996) Lipoxygenase Reaction Mechanism: Demonstration that hydrogen abstraction from substrate precedes dioxygen binding

during catalytic turnover. *Biochemistry* **35**, 12882–12892.
27 Reeder BJ, Wilson MT & Brandon J (1998) Mechanism of reaction of myoglobin with the lipid hydroperoxide hydroperoxyoctadecadienoic acid. *Biochem J* **330**, 1317–1323.
28 Knapp MJ & Klinman JS (2003) Kinetic studies of oxygen reactivity in soybean lipoxygenase-1. *Biochemistry* **42**, 11466–11475.
29 Kulkarni AP (2001) Lipoxygenase – a versatile biocatalyst for biotransformation of endobiotics and xenobiotics. *Cell Mol Life Sci* **58**, 1805–1825.
30 Romanov SG, Ivanov IV, Groza NV, Kuhn H & Myagkova GI (2002) Total synthesis of (5Z,8Z, 11Z,14Z)-18-and 19-oxoeicosa-5,8,11,14–tetraenoic acids. *Tetrahedron* **58**, 8483–8487.
31 Rapoport SM, Schewe T, Wiesner R, Halangk W, Ludwig P, Janicke-Höhne M, Tannert C, Hiebsch C & Klatt D (1979) The lipoxygenase of reticulocytes. Purification, characterization and biological dynamics of the lipoxygenase; its identity with the respiratory inhibitors of the reticulocyte. *Eur J Biochem* **96**, 545–561.
32 Normann R, Draper A, Smith H (1998) *Applied Regression Analysis*. 3rd edn. John Wiley & Sons, Inc., New York, Chichester, Weinheim, Brisbane, Singapore, Toronto.